Analogy between photorefractive oscillators and class-A lasers

K. Staliunas,* M. F. H. Tarroja,† G. Slekys,* and C. O. Weiss
Physikalisch-Technische Bundesanstalt, Bundesallee 100, 38116 Braunschweig, Germany

L. Dambly
Laboratoire de Spectroscopie Hertzienne, Universite des Sciences et Technologies de Lille, F-59655 Villeneuve d'Ascq Cedex, France
(Received 15 November 1993; revised manuscript received 31 October 1994)

Photorefractive oscillators are shown to have the same transverse properties as class-A lasers, in spite of the different mechanisms of light amplification in both systems and the different microscopic physics. A laser Ginzburg-Landau equation for the order parameter of photorefractive oscillators (PRO) is derived and correspondences between parameters of PRO's and class-A lasers are given. The close similarity between these two systems is evidenced by numerical calculations. Experimentally, a PRO is found to emit stationary patterns such as pure mode patterns and vortex lattices, and to display a periodic motion of vortices, all of which are characteristic of lasers.

PACS number(s): 42.60.Jf, 42.65.−k, 61.72.Lk

I. INTRODUCTION

In this paper we attempt to find a connection between transverse pattern formation mechanisms in photorefractive oscillators (PRO's) and other nonlinear-optical systems. The analysis in this paper shows that PRO's correspond most closely to class-A lasers. This results from analytical treatment of the PRO equations and from comparison with the laser equations, from numerical analysis, and from experiments with a $Bi_{12}SiO_{20}$ (BSO) oscillator.

We find that there are many similarities between PRO's and class-A lasers regarding the transverse properties of the optical fields in spite of different physical mechanisms of light amplification: the photorefractive crystal responds to the light intensity via the electro-optic effect [1,2] while the laser medium interacts with the optical field. The response time of the laser medium is very small compared to that of the photorefractive material (with response time between milliseconds and hours). Consequently, the spectral-gain linewidth of the photorefractive material is of the order of 1 Hz and is very small compared to that of the lasers. Furthermore, the spectral-gain linewidth of PRO's is very small compared to the cavity linewidth, which is of the order of megahertz. As shown in [3,4] this leads to an extreme frequency pulling. The emission frequency of PRO's is always close to the pump frequency (the frequency shift is of the order of 1 Hz).

Pure "resonator modes" are emitted in PRO's when spatially controlled losses (e.g., cavity misalignment, translation of an aperture off the axis of the cavity) are used [1,5]. Multimode emission patterns are often nonstationary, even with apertures restricting the number of active modes. The time dependence of the emission is often attributed to drift of the optical-cavity length [1,6–9]. These can tune the cavity modes in or out of resonance with the gain line. Nevertheless, it is possible to restrict the emission of the PRO to stationary lower-order transverse modes [5]. It was also demonstrated recently [10] that a photorefractive oscillator can be tuned, like a laser with a narrow gain line, to individual transverse-mode families. Interaction of the active modes can result in stationary patterns or mode competition or simultaneous mode emission corresponding to dynamics [10].

Several models have been formulated to describe the emission of PRO's [2–4,11,12]. In [11], e.g., a set of equations similar to those of a homogeneously broadened single-mode laser was derived and numerical simulations showed emission patterns similar to those of lasers [13]. The above models describe diffusion-type photorefractive media (whose gain is due to diffusion of electrons). In this paper, in contrast, we consider the drift mode.

In spite of the differences between PRO's and lasers, the theoretical results in [11] suggest an analogy between these two systems. In this paper, these similarities are substantiated by deriving an amplitude equation for PRO's which is isomorphic to that of class-A lasers; and by giving experimental evidence of the PRO's laserlike emission. In Sec. III, a laser Ginzburg-Landau equation (LGLE) is derived for PRO's and the correspondences between PRO and laser parameters and variables are given. The numerical results given in Sec. IV support the analogy of PRO's and class-A lasers. In Sec. V, experimental observations of the laserlike properties of a BSO oscillator are reported. In Sec. VI, the compatibility of the model with the observed behavior of the PRO with large Fresnel number is discussed.

II. MODEL FOR PHOTOREFRACTIVE OSCILLATORS

In the models for photorefractive oscillators [2–4,6,11,12], the formation of the refractive-index grating is assumed (following the initial work [14]) to result

*Permanent address: Dept. of Quantum Electronics, Vilnius University, Sauletekio av. 9, corp. 3, 2054 Vilnius, Lithuania.
†Permanent address: National Institute of Physics, University of the Philippines, Diliman, 1101 Quezon City, Philippines.

from the interference of the pump radiation and the radiation of the field oscillating in the resonator. This physical process [15] is the following. Light ionizes the atoms and the electrons drift or/and diffuse in the presence of the interference pattern. The motion of electrons results in a spatial separation of charges, and consequently in the modulation of the refractive index of the material by the linear electro-optic effect. The gain depends on the grating fringe spacing, the phase shift between the interference pattern and the refractive-index graining, and the amplitude of the refractive-index modulation. Diffusion-type crystals (e.g., $BaTiO_3$) have large-amplitude index modulation compared to drift-type crystals (e.g., $Bi_{12}SiO_{20}$). In the former type of crystals, the maximum transfer of energy from the pump beam to the generated signal occurs when the index grating is shifted $\Lambda/4$ with respect to the interference pattern (Λ is the grating period) [6,16]. This corresponds to a phase shift of $\Phi=\pi/2$. For drift-type crystals, a dc electric field is required for a higher amplitude of the refractive-index modulation. However, the phase shift in the drift mode is small and the grating moves, increasing the phase shift corresponding to optimum gain [17–20].

With optical feedback, the pump beam scattered by the imperfections of the crystal along the optical axis can initiate the oscillation process. The emission frequency is pulled by the resonator to realize the optimum combination of gain and loss.

Our starting point for the description of a PRO is the expression for the spatial profile of the refractive-index grating in the stationary case. With the total optical field and the total index of refraction given by

$$\bar{E}(\vec{r},t)=E_p(\vec{r},t)\exp(i\vec{k}_p\cdot\vec{r}-i\omega_p t)+E_r(\vec{r},t)\exp(i\vec{k}_r\cdot\vec{r}-i\omega_r t)+\text{c.c.}$$

and

$$\bar{n}(\vec{r},t)=n(\vec{r},t)\exp(i\vec{q}\cdot\vec{r}-i\Omega t)+\text{c.c.}\ ,$$

respectively, this can be written as [4]

$$n(\vec{r})=n_1\frac{E_p(\vec{r})E_r^*(\vec{r})}{I_0}\exp(i\Phi)\ . \tag{1}$$

Here $E_p(\vec{r})$ and $E_r(\vec{r})$ are the envelopes of the pump and signal field and $n(\vec{r},t)$ is the envelope of the refractive-index grating. $\Omega=\omega_p-\omega_r$ and $\vec{q}=\vec{k}_p-\vec{k}_r$. $\vec{r}=(x,y)$ is the coordinate in the transverse plane: there is no dependence on the longitudinal coordinate due to the mean-field approximation. I_0 is the intensity of the total optical field in the photorefractive material: $I_0=|E_p(\vec{r})|^2+|E_r(\vec{r})|^2$. It is assumed that the signal is small compared to the pump, $|E_r(\vec{r})|\ll|E_p(\vec{r})|$, and the pump is undepleted. n_1 is the amplitude of the refractive-index grating and Φ is the phase shift between the refractive-index grating and the interference pattern. The values n_1 and Φ depend among other things on the frequency Ω: the expression for n_1 and Φ is [3,4,14,17]

$$n_1(\vec{r},\Omega)\exp[i\Phi(\vec{r},\Omega)]=\frac{n_s}{1-i\Omega/\gamma}\exp(i\Phi_0)\ . \tag{2}$$

Here n_s is the saturated value, and γ is the decay rate of the refractive-index grating (γ is usually of order of a magnitude of 1 s^{-1}; n_s depends on the dc voltage applied). Φ_0 is related to the local response of the crystal under illumination [4,17]. For diffusion-type photorefractive material $\Phi_0=\pi/2$. Here drift-type material is considered; thus Φ_0 is small. $\Phi_0=0$ is therefore assumed.

The equation for the generated optical field is derived in the paraxial approximation for a resonator with curved mirrors [3,11,12]. The field is fed by the pump field which is scattered from the index grating. The equation for the generated field in the mean-field approximation is

$$\frac{\partial E_r}{\partial t}=\kappa\left[-(1+i\beta)E_r+i\Delta\omega_\perp\left[\frac{\vec{\nabla}^2}{4}-r^2\right]E_r+iE_p n^*\right]\ . \tag{3}$$

Here κ is the photon decay rate (usually of order of magnitude 10^8 s^{-1} and thus $\gamma\ll\kappa$). β is the resonator frequency detuning from the gain line center, $\Delta\omega_\perp$ is the frequency separation between transverse-mode families of the empty resonator,

$$\vec{\nabla}^2=(1/r^2)(\partial^2/\partial\phi^2)+(1/r)(\partial/\partial r)+\partial^2/\partial r^2$$

is the Laplace operator in the plane normal to the optical axis of the PRO, and (r,ϕ) are the polar coordinates in this plane. The spatial coordinates are normalized to the radius of the fundamental Gaussian (TEM_{00}) mode of the resonator, and the frequencies β and $\Delta\omega_\perp$ in (3) are normalized to the width of the TEM_{00} mode resonance.

To determine Ω and Φ a plane-mirror-cavity case is considered for simplicity. Then Eq. (3) takes the form

$$\frac{\partial E_r}{\partial t}=\kappa[-(1+i\beta)E_r+id\vec{\nabla}^2E_r+iE_p n^*]\ . \tag{4}$$

Here $d=\lambda L/(4\pi T)$ is the diffraction coefficient. The spatial coordinates are in this case not normalized to the radius of a beam waist but to the wavelength λ of the radiation. L is the round-trip length of the resonator, and T is the total round-trip loss of the PRO. We search for a stationary solution of (1), (2), and (4) in the form of a tilted wave [21] $E_r(r)=E_0\exp(i\vec{k}\cdot\vec{r})$, which leads to

$$\frac{|E_0|^2}{|E_p|^2}=\frac{-in_s}{(1-i\Omega/\gamma)[1-i(\beta+dk^2)]}-1\ . \tag{5}$$

Since the right-hand side of (5) is real $(\beta+dk^2)\Omega/\gamma=1$. The intensity of the generated field $|E_0|^2$ is maximal when $\Omega=\gamma$, as seen from (5). This means that the phase shift Φ is $\Phi=\arctan(\Omega/\gamma)=\pi/4$ for drift-type photorefractive material (different from diffusion-type materials). The detuning is $\beta=1-dk^2$, and the intensity of the generated field at this optimum frequency shift is $|E_{\max}|^2/|E_p|^2=(n_s/2-1)$.

The condition of maximum gain leads to "frequency-shift" phenomena in drift-type PRO's. Indeed the zero-mode $|\vec{k}_0|^2=0$ is maximally amplified for nonzero detuning $\beta=1$. In lasers and diffusion-type PRO's there is no such frequency shift, and there the transverse wave num-

ber of the generated wave is proportional to negative detuning: $|\vec{k}|^2=-\beta/d$.

Due to the slow response of the photorefractive material, the refractive-index grating builds and decays with a time delay with respect to the optical interference pattern. The low time variation of the refractive-index profile has been previously analyzed [2,11,12]. We derive the time-dependent equation for the refractive-index profile directly from (1) and (2), which actually are the expressions for the Fourier components $n(\Omega)$. Multiplying both sides of (1) by $(1-i\Omega/\gamma)$ and using the inverse Fourier transform to convert to the time domain, one obtains

$$\frac{\partial n}{\partial t}=-\gamma\left[n-i\frac{\Omega}{\gamma}n-n_s\frac{E_pE_r^*}{I_0}\right]. \tag{6}$$

[In all equations the particular reference frequency $\omega_{\text{ref}}=\Omega$ is used. Consequently, (1) and (2) are rewritten with $\omega_{\text{ref}}=0$, then the inverse Fourier transformation is carried out, and finally $\omega_{\text{ref}}=\Omega$ is again reintroduced to obtain (6).]

Taking into account that $\Omega/\gamma=\tan(\Phi)=1$, and normalizing the amplitude of the generated field to the pump field, $E(\vec{r},t)=E_r(\vec{r},t)/E_p(\vec{r})$, Eq. (6) transforms to

$$\frac{\partial n}{\partial t}=-\gamma\left[n-in-n_s\frac{E^*}{1+|E|^2}\right]. \tag{7}$$

Using the same normalization of the optical field one obtains from (3)

$$\frac{\partial E}{\partial t}=\kappa\left[-(1+i\beta)E+i\Delta\omega_\perp\left[\frac{\vec{\nabla}^2}{4}-r^2\right]E+in^*\right]. \tag{8}$$

The system of equations (7) and (8) is the basis for the analysis of the field dynamics of the PRO.

III. ANALOGY WITH CLASS-A LASERS

The similarity with class-A lasers is shown in the following by adiabatic elimination of the fast-relaxing optical field from (7) and (8). The envelope of the refractive-index grating is expressed for this purpose in terms of the optical field in Eq. (8) (assuming $\partial E/\partial t=0$):

$$n=i\left[1-i\beta+i\Delta\omega_\perp\left[\frac{\vec{\nabla}^2}{4}-r^2\right]\right]E^*. \tag{9}$$

Substituting (9) into (7) and letting the differential operator $[1+i\beta-i\Delta\omega_\perp(\vec{\nabla}^2/4-r^2)]^{-1}$ act on both sides of (7) yields

$$\frac{\partial E}{\partial\tau}=-E(1+i)+\frac{in_s}{1+i\beta-i\Delta\omega_\perp(\vec{\nabla}^2/4-r^2)}\frac{E}{1+|E|^2}. \tag{10}$$

Here $\tau=t\gamma$ is a normalized time.

Equation (10) is similar to the class-A laser equation in [21,22]. In the case of a resonator with plane mirrors, (10) reduces to

$$\frac{\partial E}{\partial\tau}=-E(1+i)+\frac{in_s}{1+i\beta-id\vec{\nabla}^2}\frac{E}{1+|E|^2}, \tag{11}$$

where d is the diffraction coefficient, as defined in Sec. II.

Equation (11) was derived by adiabatic elimination of the fast-relaxing variable of the optical field, but it is written in terms of this enslaved variable (instead of the refractive index) to show the similarity with the class-A laser amplitude equation. This is possible since the enslaved optical field is an explicit function of refractive index, and vice versa.

The stationary solution of (11) is $E(\vec{r},t)=E_0\exp(i\vec{k}\cdot\vec{r})$, where $E_0=n_s/2-1$ and $d|\vec{k}|^2=1-\beta$. This means that certain spatial modes with spatial wave numbers $|\vec{k}|$ proportional to the resonator detuning are favored, taking into account the linear frequency shift. (This is similar to a laser [21] except for the frequency shift.) In the case of a resonator with spherical mirrors (10) certain transverse modes are favored correspondingly. Analysis of (11) shows an amplification profile of Lorentzian shape in the optical frequency domain as well as in the spatial wave-number domain. (As shown in [22,23] the gain profile in the frequency domain corresponds precisely to that of the spatial wave numbers for lasers.)

The half-width of the oscillation frequency range of the PRO calculated from (11) is $\Delta\beta^2=n_s-2=2|E_0|^2$. ($\Delta\beta$ is the maximal detuning at which a particular mode is still above threshold.) The half-width $\Delta\beta$ of the PRO is equal to the half-width of the oscillation range of lasers. The $\Delta\beta$ of the PRO is determined by the spectral width of the empty-resonator mode to which all frequencies are normalized (e.g., the TEM_{00} mode), and by n_s, which corresponds to the pump.

Further, the differential operator in (11) is expanded in a Taylor series:

$$\frac{in_s}{1+i\beta-id\vec{\nabla}^2}=\frac{in_s}{(1+i)+i(\beta-d\vec{\nabla}^2-1)}$$

$$\cong(1+i)(n_s/2)[1-(1+i)(\beta-d\vec{\nabla}^2-1)/2+i(\beta-d\vec{\nabla}^2-1)^2/4+\cdots]. \tag{12}$$

This expansion is well justified if the condition $\varepsilon=\beta-d\vec{\nabla}^2-1\ll1$ is fulfilled. The analysis of (10) and (11) shows that this is the case for generation near the threshold, when $|E|\ll1$ (or $|E_r|\ll|E_p|$). For larger pump and larger intensities of generated radiation of the condition of smallness of ε holds only approximately (i.e., $\varepsilon\leq1$). The Taylor expansion (12) means that the Lorentzian shape of the gain line is replaced by a parabolic one. This leads, in general, to an additional filtering of the transverse wave numbers far from the gain-line maximum.

The expansion (12) truncated at the second-order term and inserted into (11) leads to the following equation:

$$\frac{\partial E}{\partial \tau}=\left[\frac{n_s}{2}-1\right](1+i)E-i\frac{n_s}{2}(\beta-d\vec{\nabla}^2-1)E$$
$$+I(i+1)\frac{n_s}{8}(\beta-d\vec{\nabla}^2-1)^2E-\frac{n_s}{2}(1+i)\mathcal{X}$$
$$+i\frac{n_s}{2}(\beta-d\vec{\nabla}^2-1)\mathcal{X}-i(i+1)\frac{n_s}{8}(\beta-d\vec{\nabla}^2-1)^2\mathcal{X}\ . \tag{13}$$

Here $\mathcal{X}=E|E|^2/(1+|E|^2)$ is small ($\mathcal{X}\ll E$) near the generation threshold. Retaining in (13) only the terms of leading order [the term $(\beta-d\vec{\nabla}^2-1)E$ is of the same order of smallness as $\mathcal{X}$], Eq. (13) is simplified to

$$\frac{\partial E}{\partial \tau}=\left[\frac{n_s}{2}-1\right](1+i)E-i\frac{n_s}{2}(\beta-d\vec{\nabla}^2-1)E$$
$$-\frac{n_s}{8}(\beta-d\vec{\nabla}^2-1)^2E-(1+i)E|E|^2\ . \tag{14}$$

Here the cubic approximation

$$\mathcal{X}=E|E|^2/(1+|E|^2)=E|E|^2 2/n_s$$

is used to simplify the nonlinear term in (14). In case of curved mirrors Eq. (14) transforms to

$$\frac{\partial E}{\partial \tau}=\left[\frac{n_s}{2}-1\right](1+i)E-i\frac{n_s}{2}\left[\beta-\Delta\omega_\perp\left[\frac{\vec{\nabla}^2}{4}-r^2\right]-1\right]E$$
$$+\frac{n_s}{8}\left[\beta-\Delta\omega_\perp\left[\frac{\vec{\nabla}^2}{4}-r^2\right]-1\right]^2E-(1+i)E|E|^2\ . \tag{15}$$

Equations (14) and (15) are the same laser Ginzburg-Landau equation that has been derived for class-A lasers in [21,22]. This indicates that the transverse-field dynamics in PRO's and class-A lasers are similar.

We note that the analogy between PRO's and class-A lasers may be also shown without referring to the LGLE (15). The transverse-mode expansion of (7) and (8) and the adiabatic elimination of the fast variable of the optical field leads to

$$\frac{\partial f_i}{\partial \tau}=-\gamma\left[f_i\left[1+\frac{\Omega}{\gamma}\right]-\frac{in_s}{1+i\beta+i\omega_i}\times\int_0^{2\pi}d\phi\int_0^{\infty}\rho\,d\rho\,A_i^*\frac{E}{1+|E|^2}\right]\ . \tag{16}$$

Here $f_i(\tau)$ and ω_i are the amplitudes and eigenfrequencies of the resonator modes $A_i(\vec{r})$. On the other hand, the equation for mode amplitudes of a class-A laser is [24]

$$\frac{\partial f_i}{\partial \tau}=-\kappa\left[f_i[1+i(\omega_i-\omega)]-\frac{2C}{1+i(\omega_a-\omega)\kappa/\gamma_\perp}\times\int_0^{2\pi}d\phi\int_0^{\infty}\rho\,d\rho\,A_i^*\frac{E}{1+|E|^2}\right]\ . \tag{17}$$

Here ω_a is the atomic frequency and ω is the unknown laser frequency. The frequencies β, $\Delta\omega_\perp$, ω_i, ω_a, and ω in (16) and (17) are scaled with the cavity linewidth κ.

Equations (16) and (17) are similar, and in the single-mode case are identical (except for the frequency shift and pulling). In the general multimode case a difference arises, which is due to the additional self-defocusing [the imaginary part of the nonlinear term in (15)] of PRO's absent for class-A lasers.

The results of a numerical integration of the full set of PRO equations (7) and (8) and of the LGLE's (14) and (15), as well as of the full Maxwell-Bloch equation system for Class-A lasers, are given in the next section. The comparison of numerical results confirms the validity of the LGLE for PRO's and the equivalence of PRO's and class-A lasers.

The following correspondences are found between parameters for the two systems.

(i) The pump parameter of the lasers D_0 corresponds to $n_s/2$ of PRO's. In drift-type PRO's, the dc field corresponds to the pump in real lasers since n_s is directly proportional to the dc field.

(ii) The detuning in lasers corresponds to $\beta'=\beta-\Omega/\gamma=\beta-1$ for PRO's. This means that selection of transverse-mode families can occur through resonator tuning as in lasers. The difference with the laser is that a PRO detuning is smaller by $\Delta\beta=1$ than for a laser to excite the same transverse-mode family (the frequency shift).

(iii) Mode beats are on a very slow time scale. The frequency $\Delta\omega_{\text{beat}}=\Delta\omega_\perp\gamma/\kappa$, since the time in (14) and (15) is scaled. This was also found in [3,11,12] and interpreted in terms of frequency pulling.

(iv) There is a transverse-mode selection in PRO's analogous to that of lasers. This selection occurs for lasers when the spectral width of the gain line is narrower than the free spectral range of the resonator. In the PRO the selection occurs not by the finite gain linewidth, but by the finite width of the empty-resonator modes. For simultaneous oscillation of several transverse modes, it is necessary (but not sufficient) that the linewidths of the resonator modes overlap. Mathematically the terms of fourth-order diffusion in (14) and (15) are responsible for transverse-mode selection in lasers and PRO's.

There is one important difference between PRO's and class-A laser: the imaginary part of the nonlinear term [e.g., in (14) and (15)] causes self-defocusing. This can influence the dynamics when at least a few transverse-mode families are active. Then the self-defocusing could cause a transfer of energy to the lower-transverse-mode families. In the case of emission within only one transverse-mode family, the defocusing plays no role,

which also follows from comparison of (16) and (17).

It follows the the PRO behaves like a "very slow" class-A laser and with additional self-defocusing and frequency shift. In the case of only one active transverse-mode family (the case studied experimentally in this paper) the PRO behaves completely identically to a class-A laser.

IV. NUMERICAL COMPARISON OF PRO'S WITH LASERS

A numerical integration of PRO equations (7) and (8), of LGLE's (14) and (15), and of the full set of Maxwell-Bloch equations for the class-A laser case (e.g., in the form of those in [22,23]) was made, in order to verify the equivalence of PRO's and class-A lasers. Integration was done for the case of only one spatial dimension, since it allows one to compare the result with higher accuracy for limited computing time. The split-step method has been used, where the nonlinear terms were calculated in the space domain, and the Laplace operator in the Fourier domain.

Tunability. The intensity and the frequency of emitted radiation of a PRO dependent on detuning are given in Figs. 1(a) and 1(b) as calculated from (7) and (8). The tunability is evident from the amplitude dependence Fig. 1(a). The emission frequency is equal to the mode frequency when a mode is tuned precisely to the gain line, as seen from Fig. 1(b). The emission frequency depends linearly on the detuning near the central frequency of the mode, in correspondence with (15). For larger detunings a deviation from the linear dependence is seen: it is related to the higher- (second-) order diffraction term omitted in going from (13) to (14) [the imaginary part of the second-order diffusion term in (13)].

Coexistence and competition of modes. It is known [25] that the neighboring transverse modes do not coexist in class-A lasers in the one-dimensional (1D) case (the spatial overlap of intensities of neighboring transverse modes is larger than the coexistence threshold for class-A lasers). This leads to hysteresis in the tuning curve as shown in Fig. 1(c). The situation is completely different for class-B lasers where the neighboring modes coexist simultaneously and beat [Fig. 1(d)]. Our numerical calculations show that the hysteresis in the tuning curve of PRO's [Figs. 1(a) and 1(b)] is very similar to that of class-A lasers. Also, the transition between neighboring transverse modes has been analyzed numerically for class-A and -B lasers (see Fig. 2), and compared to that of PRO's. The transition for PRO's is the same as for class-A lasers.

The frequency shift. The comparison of Figs. 1(a) and 1(b) with Figs. 1(c) and 1(d) shows that the excitation of a particular transverse mode occurs for different detunings for lasers and PRO's. The difference of detunings is constant: $\Delta\beta=1$ for all transverse modes. This illustrates the frequency-shift phenomenon of drift-type PRO's.

The phase shift. PRO equations (7) and (8) are invariant with respect to the reference phase shift between the refractive-index grating and light interference pattern: the system chooses the "correct" phase shift and correct

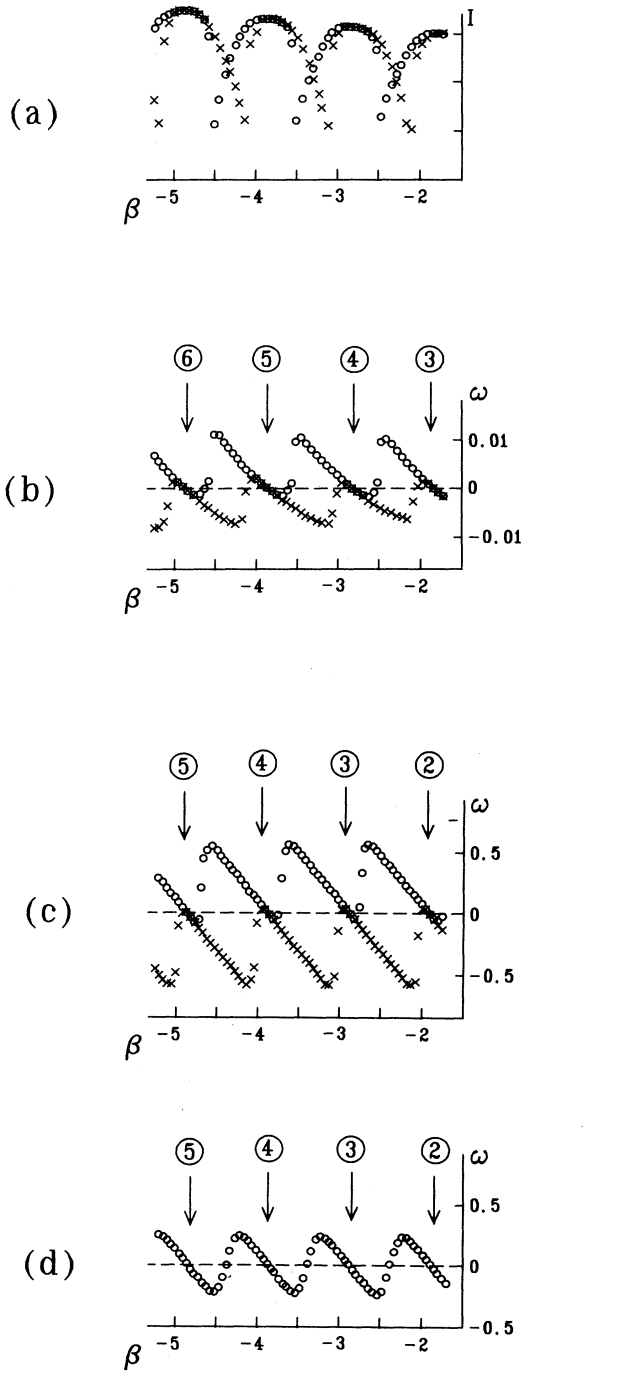

FIG. 1. Tuning curves for PRO's [(a) and (b)] for class-A lasers (c), and class-B lasers (d) in the 1D case. The total power emitted (a) and its frequency (b) depending on the resonator detuning β are calculated by numerical integration of (7) and (8). The laser frequency dependencies (c) and (d) were calculated by numerical integration of the full set of Maxwell-Bloch equations (in a form used in [22,23]). The crosses correspond to the variation of β towards larger values and the circles towards smaller values of β. $\Delta\omega_\perp=1$; other parameters: $n_s=3$, $\gamma/\kappa=0.01$ for PRO [(a) and (b)], $D_0=1.5$, $\gamma_\perp/\kappa=3.5$, $\gamma_\parallel/\kappa=3.5$ for class-A lasers (c), and $D_0=1.5$, $\gamma_\perp/\kappa=3.5$, $\gamma_\parallel/\kappa=0.2$ for class-B lasers (d). Power increases with negative detuning due to the larger volume of the higher transverse modes.

frequency independent of this reference phase shift Φ. If a value of Φ different from its "correct" value $\Phi=\pi/4$ is used in (7) it only changes the frequency of the solution. Equations (7) and (8) were numerically integrated with values of Φ different from its "correct" value and the radiation frequency at the central frequency of the mode closest to resonance was calculated. Figure 3 shows the dependence of the radiation frequency on the value of the phase Φ. It is evident that the optimum value of the phase is $\Phi=\pi/4$ in correspondence with the theoretical analysis.

Standing-wave (SW) and traveling-wave (TW) patterns. It is known that a stationary SW pattern is emitted by class-A lasers slightly above threshold [23]. At a particular value of the pump the symmetric SW pattern is changed to an asymmetric TW pattern. Figure 4 shows the transverse distributions of the optical field for different values of the pump: a SW (or Hermite mode) pattern near the threshold [Fig. 4(a)], the pattern dominated by a TW for large values of the pump [Fig. 4(c)], and the pattern for intermediate values of the pump [Fig. 4(b)]. The comparison of Fig. 4 with the patterns calculated for class-A lasers in [23] shows the good correspondence.

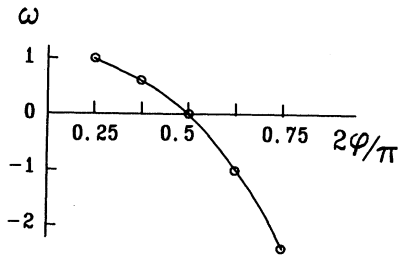

FIG. 3. Frequency of the fifth 1D Hermite mode at the detuning corresponding to the maximum of its intensity, for different values of phase shift, as given by numerical integration of (7) and (8). [The linear term $n(1-i)$ has been substituted by a general one: $n[1-i\tan(\Phi)]$ in (7).] Other parameters as in Fig. 2.

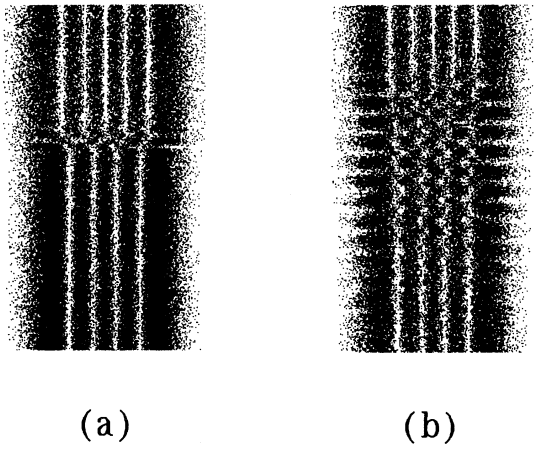

FIG. 2. Evolution of the emitted 1D pattern as detuning is varied from $\beta=-10$ (top of the figure) to $\beta=-8$ (bottom) for class-A (a) and class-B (b) lasers, and for PRO's (c). The horizontal axis corresponds to the spatial coordinate; time continuously changes along the vertical coordinate over the value $\Delta t=25$ from top to bottom. $\Delta\omega_\perp=2$; $D_0=2$ (pump value) [$n_s=4$ in (c)]; other parameters as in Fig. 1.

Standing-wave–traveling-wave transition. A convenient parameter to characterize the spatial pattern of a laser, and to distinguish between the SW- and TW-dominated patterns is

$$\vec{K}=\frac{\int \vec{k}|E(\vec{k})|^2 d\vec{k}}{\int |\vec{k}||E(\vec{k})|^2 d\vec{k}} . \tag{18}$$

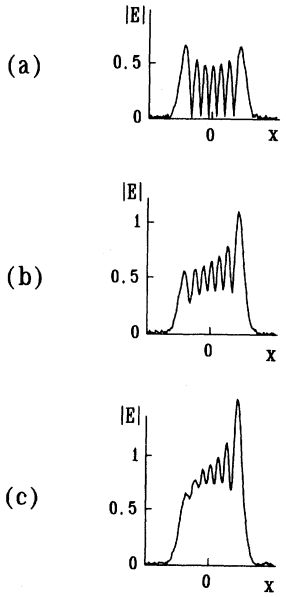

FIG. 4. Transition from standing to traveling wave of a PRO in the 1D case. Stationary transverse patterns for different values of n_s: (a) $n_s=2.25$, (b) $n_s=2.75$, (c) $n_s=3.25$. $\beta=-5.2$; other parameters as in Fig. 1.

Here the spatial spectrum $E(\vec{k})$ is calculated by integration over the whole laser cross section (here over the whole 1D space), or over all limited range. $\vec{K}$ is then the average tilt of the laser beam with respect to the optical axis, or of part of the beam, depending on the integration limits. The numerically calculated dependence of the time-averaged value of $|\vec{K}|$ of the PRO on the pump is shown in Fig. 5, where the transition between SW- ($T\sim 0$) and TW-dominated patterns ($T\sim 1$) can be seen.

The SW-TW transition is characteristic for class-A lasers, as seen from Fig. 5(b) (crosses). For class-B lasers transverse dynamics sets in before the SW-TW transition occurs. The error bars in Fig. 5(b) indicate the nonstationarity of this T parameter for class-B lasers.

Defocusing. A numerical test of self-defocusing in (14) and (15) was made by calculating the spatial size of an emitted mode (fifth 1D Hermite mode): The self-defocusing causes an increase of mode width. (Self-defocusing also influences the dynamics, but the quantitative characterization of the influence on the dynamics is complicated.) For the purpose the mode width was calculated for different values of the self-defocusing parameter in (15), by replacing the nonlinear term $(1+i)E|E|^2$ in (15) by a generalized one $(1+ic)E|E|^2$ and varying the parameter c. The results are given in Fig. 6: comparison with the spatial width of the mode calculated from (7) and (8) yields the value of the self-defocusing parameter $C=1.00\pm 0.05$, in good agreement with the analytically obtained value of $c=1$.

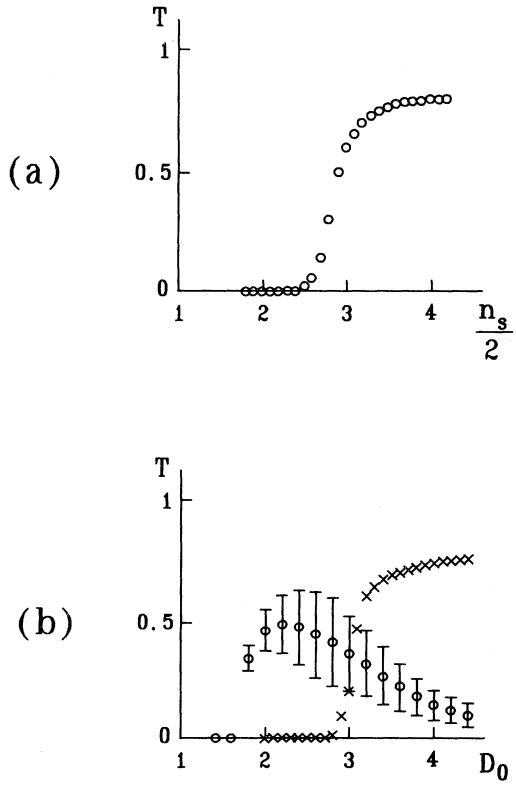

FIG. 5. Value of asymmetry parameter (tilt T) for PRO (a), class-A laser [(b), crosses], and class-B laser [(b), circles with error bars] depending on the control parameters n_s and D_0, respectively. Circles indicate the average tilt and error bars the variance of T. Other parameters as in Fig. 1.

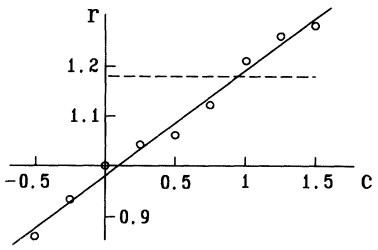

FIG. 6. Width of the fifth 1D Hermite transverse mode depending on the parameter c of self-focusing as obtained by numerical integration of (15) (circles). The width is normalized to the mode width in the case of no self-focusing or -defocusing. The dashed line corresponds to the mode width as calculated by integrating (7) and (8) ($r=1.185$). The parameters are $\Delta\omega_\perp=2$, $\beta=-9$, $n_s=8$, and $\gamma/\kappa=0.01$.

V. EXPERIMENT

The $Bi_{12}SiO_{20}$ oscillator used consists of the active crystal, two plane mirrors, and two curved mirrors in a folded-ring resonator configuration as shown in Fig. 7. The BSO crystal is placed close to one of the curved mirrors in an orientation so that the electric field lies in the $\langle 001\rangle$ crystalographic axis and the pump beam of 514.5 nm wavelength from a single-mode Ar laser propagates in the $\langle \bar{1}10\rangle$ direction. The electric field is along the $\langle 110\rangle$ axis. The gain of the photorefractive medium is unidirectional and thus the generated light propagates with the pump.

Mirror M_2 has 15% transmission which allows one to observe the field generated. Mirror M_1 is 5% transmitting to allow injection of a reference beam into the resonator in the direction opposite to that of the propagation of the generated beam. This reference beam is used to measure the transmission of the resonator at the pump frequency for the purpose of active stabilization of the resonator length. Because of the small intensity, perpen-

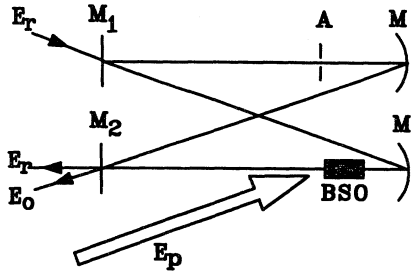

FIG. 7. Schematic diagram of the experimental setup. M_1, M_2, and M are resonator mirrors, A the aperture, E_0, E_p, and E_r the generated field, pump field, and reference field, respectively.

dicular polarization, and propagation in the direction opposite to that of the pump beam, the reference beam does not affect the light amplification.

The angle between the pump beam and the oscillator axis was chosen close to 1° for optimum gain (which was found from gain measurements with a moving grating as described in [17–20]). The pump-beam intensity used is typically 10 mW/cm^2. The dc field is set to only 8.0 kV/cm so that the gain is low enough to allow the emission of pure resonator modes when an aperture of sufficiently small diameter restricts the resonator Fresnel number.

The generated radiation coupled through mirror M_2 is recorded by a charge-coupled device (CCD) camera. To detect phase singularities or vortices, the radiation beam can be superposed at a small angle with a uniform (expanded) beam from the pump laser. This produces dislocations in the interference fringe pattern where phase singularities are located [26,27].

With the ring-resonator length of 2.1 m and 1.5 m radii of curvature of the curved mirrors, the longitudinal- and transverse-mode frequency separations are 140 and 57 MHz, respectively. The beam waist of the TEM_{00} mode is 108 μm. With the crystal loss of $\alpha = 1.0$ cm^{-1} and in the absence of a limiting aperture, the resonator linewidth [full width at half maximum (FWHM)] is ~ 50 MHz. The number of active modes is controlled by the aperture inside the resonator. Transverse-mode frequencies within one free spectral range of the empty resonator are schematically shown in Fig. 8.

For resonator tuning, one of the curved mirrors is mounted on a piezotranslator. The passive resonator transmission can be monitored through M_2 using the reference beam which is injected into the oscillator through mirror M_1. Due to the large crystal loss, the finesse of the empty resonator is only ~ 1 and thus the resonances of the longitudinal modes overlap in frequency space. The transverse modes are consequently not resolved. The observed change of resonator transmission, as the cavity length is varied, is only 20% as shown in Fig. 8. This small variation of transmission is, however, sufficient to distinguish between different points within a free spectral range (Fig. 8).

The PRO can be made to emit in one or another transverse-mode family by changing its resonator length. In this way sequences of transverse-mode emission can be explored for different diameters of the internal aperture when the resonator length is changed.

When the aperture is sufficiently small (diameter d less than 1 mm), only the fundamental mode TEM_{00} is active. The maximum power occurs as expected at a resonator length where the reference-beam transmission is also maximal. The scan of the cavity length within one free spectral range in this case results only in a change of the intensity of the TEM_{00} mode.

The emission of $q = 1$ modes occurs when the aperture is increased ($d = 1$ mm). Then the emission in the $q = 0$ mode can change to emission in the $q = 1$ mode family, while the resonator length is scanned. There is a region of the resonator length where there is no emission. This is as in class-A lasers where the overlap of resonator-mode profiles is not sufficient for simultaneous emission of modes if the pump is not large enough [25,24]. When the aperture diameter is increased sufficiently to allow emission up to modes of transverse order $q = 3$, the sequence of mode families 0,3,1,2,0 is expected; $q = 3$ belonging to the adjacent longitudinal free spectral range. The observed sequence as shown in Fig. 9 confirms this. TEM_{00}-mode emission is observed around the resonator

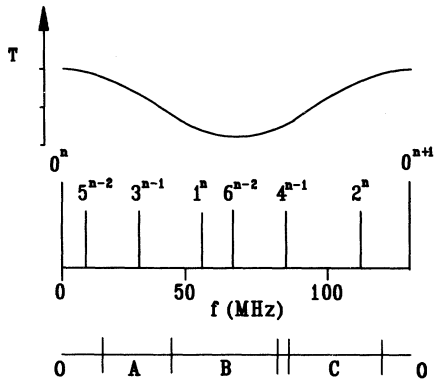

FIG. 8. PRO resonator mode spectrum corresponding to Fig. 7. q^n signifies transverse-mode order q and longitudinal order n. The transmission T of the reference beam is also shown. O, A, B, and C indicate regions of oscillation of mode families q equal to 0, 3, 1, and 2, respectively, when the aperture allows oscillation only up to the $q = 3$ family.

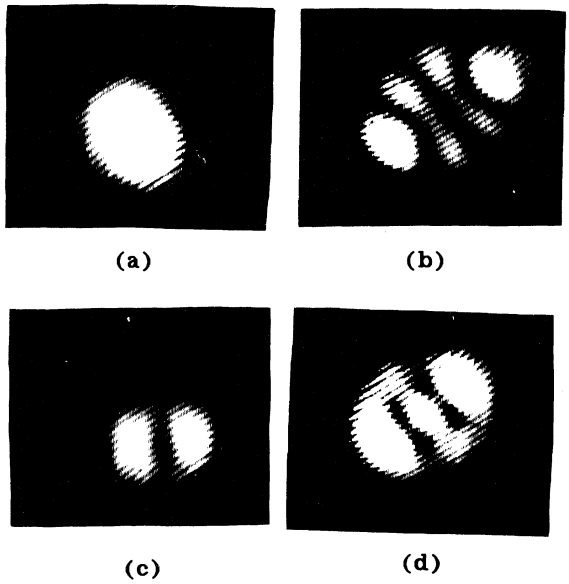

FIG. 9. Sequence of patterns observed when the resonator length is changed through one free spectral range (mode families up to $q = 3$ are allowed to oscillate). Only one representative pattern for each mode family is shown. (a) $q = 0$, (b) $q = 3$, (c) $q = 1$, and (d) $q = 2$. The fringes are due to interference with the pump beam (superimposed to detect vortices).

length at the maximum transmission of the reference beam (Point O in Fig. 8). Emissions corresponding to $q=3$, 1, and 2 are observed in regions A, B, and C, respectively. Furthermore, a narrow region with no emission is observed between B and C. This is due to the relatively large frequency separation between 1^n and 2^n (see Fig. 8) compared with that of other pairs of adjacent modes (for example, between 0^n and 3^{n-1} or between 2^n and 0^{n+1}). For larger apertures, other mode families can be emitted. For $d=1.2$ mm, modes up to $q=4$ are observed in the sequence 0,3,1,4,2,0 consistent with Fig. 8. The expected sequence of modes up to $q=5$ is also observed. As the aperture is further opened the number of oscillating-mode families is increased, and the spacing between mode families becomes small. Mode interaction as well as resonator-length drifts do not allow us then to unambiguously observe the sequences of emission of modes as the resonator length is changed.

It is a common observation that the transverse-intensity distribution of PRO field changes randomly in time (e.g., from one mode or combination of modes to another) even when no intentional change of resonator length is made [1,5,7–9]. It may be expected that this is due to mechanical and/or thermal fluctuations of the resonator length. To distinguish dynamical effects from such technical ones, an active stabilization which can lock the resonator length to one corresponding to an extremum (i.e., minimum or maximum) of the reference transmission was used. This stabilization scheme has to handle changes of the PRO resonator length as well as pump-frequency fluctuations. A length stabilization of the PRO resonator alone is not sufficient. Since the "gain line" of the PRO is practically at the pump frequency, a control of the PRO resonator length with reference to the pump frequency controls both pump-frequency and PRO resonator-length fluctuations as required.

When the resonator is frequency stabilized, only modes which correspond to the stabilized resonator length are observed. Without stabilization, the oscillator does emit all modes of the resonator which are not suppressed by the aperture.

For an aperture diameter of 1 mm, the intensity of the TEM_{00} mode is stable when the resonator length is stabilized to the maximum (Fig. 8) of the reference transmission. Modes of the family $q=1$ are the only ones emitted when the resonator is stabilized to the minimum of the reference transmission. In the latter case the hybrid TEM_{01}^{*} "doughnut mode" is emitted. In the presence of astigmatism of the cavity, the constituent Hermite modes TEM_{01} and TEM_{10} have different emission frequencies and beating between these modes can occur. This beating within the $q=1$ family ("unlocked doughnut") corresponds to an alternating emission between Hermite modes of orthogonal orientation and "doughnut" modes of opposite helicities [28,29]. Because of the very small polarization decay rate, the oscillating modes are strongly frequency pulled towards the gain line center of the material. Consequently in the "unlocked doughnut" case the difference of frequencies of the active constituent modes is of the order of 1 Hz. Thus alternation between the four mentioned patterns shown in Fig. 10 occurs with

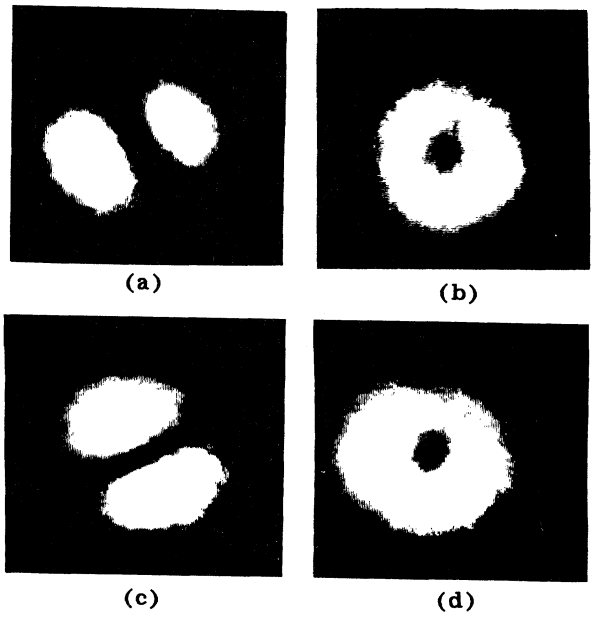

FIG. 10. The "unlocked doughnut." Output alternates between (a) Hermite 01 mode, (b) right-hand helical wave, (c) Hermite 10 mode, and (d) left-hand helical wave.

~1 Hz period.

Alternation between patterns of higher-mode families (e.g., $q=2$) is also observed. As [10] suggests, this can also be used by astigmatism, which lifts the degeneracy between modes of the same family.

When the frequency separation between adjacent transverse-mode families is small, simultaneous oscillation of different mode families can occur. The dynamical patterns corresponding to the beating of these modes are then observed.

These simultaneous oscillations can manifest themselves in "spinning vortices" (also observed in class-A lasers [24]). Several vortices move then on a circle around the optical axis. These spinning vortices appear when patterns with multiply charged phase singularities are simultaneously oscillating with a TEM_{00} mode. Spinning vortices were observed here for aperture sizes which allow the simultaneous emission of the $q=2$, 3, or 5 mode family and the fundamental mode. Correspondingly, two spinning vortices [Fig. 11(a)] were observed which correspond to the beating of 2^n and 0^{n+1} modes in Fig. 8. Similarly, in the region between $q=0$ and $q=3$, three spinning vortices are observed [see Fig. 11(b)]. For a larger aperture ($d=1.5$ mm), five spinning vortices [Fig. 11(c)] are observed, corresponding to the simultaneous oscillation of 0^n and 5^{n-2} modes. The frequency of rotation of the spinning vortices in all three cases is of the order of 1 Hz. Similarly, and for a slightly larger aperture, simultaneous oscillation of the doughnut mode and a mode of family $q=6$ is observed, corresponding to the minimum of the reference transmission (Fig. 12).

The motion of vortices on a 1 Hz time scale occurs due

to the beating between modes which are frequency pulled proportionally to γ/κ (as discussed above). Hence such dynamics, which can only be indirectly measured in lasers as the speeds are too high for 2D recordings, can be observed here visually or recorded by ordinary video equipment. In view of this slowing of the dynamics and the equivalence with class-A lasers, we might call PRO's "slow-motion lasers," and use them generally as model systems to explore class-A laser physics.

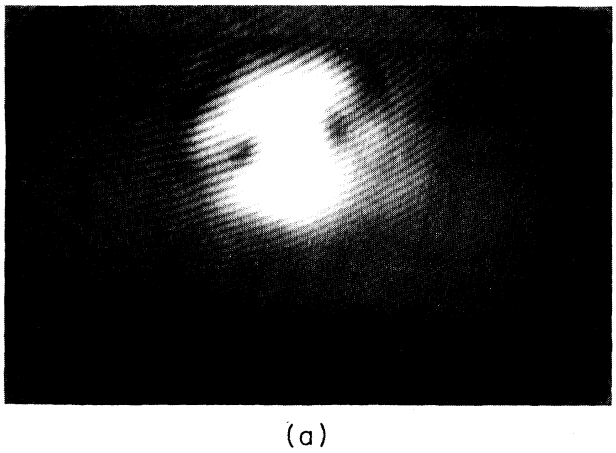

FIG. 11. Circling about the optical axis of (a) two vortices, (b) three vortices (indicated by arrows), and (c) five vortices. For (a) and (b) the emitted field is superimposed on part of the pump radiation to detect vortices.

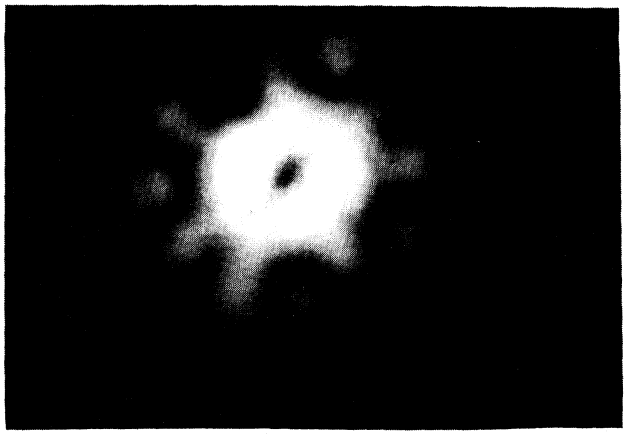

FIG. 12. Simultaneous emission of a $q=1$ "doughnut mode" and a pattern of the $q=6$ mode family.

For an even larger aperture ($d=2.5$ mm), a stationary "vortex crystal" is observed as shown in Fig. 13. It is built of positively and negatively charged singularities in the fashion of a two-dimensional ionic crystal. This latter phenomenon has been observed in class-A lasers [30,31]. Its existence and stability has also been predicted for large-area class-A lasers [23].

Finally, no relaxation oscillations were observed in PRO's. This may be considered as experimental evidence of the equivalence of a PRO with a class-A laser rather than with the class-B laser.

VI. DISCUSSION

The correspondence between the PRO and class-A laser has been shown, particularly for cases of only a few

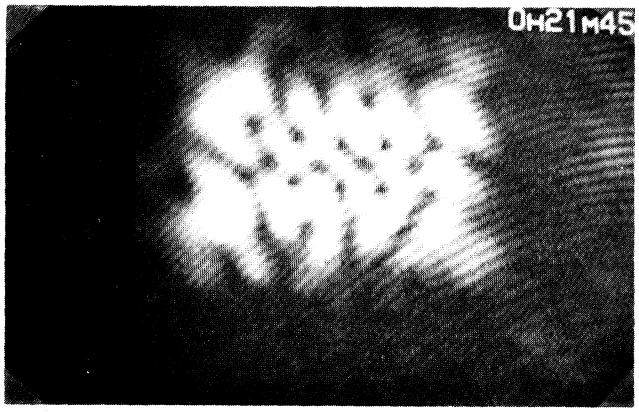

FIG. 13. A "vortex crystal." The fringes are due to interference with part of the pump beam (superposed to detect vortices).

active transverse-mode families. Like a narrow-gain-line laser, a PRO can be tuned from one transverse-mode family to another by changing the resonator length. Patterns such as "spinning vortices," astigmatism-induced pattern alternation, and "vortex crystals" typical for class-A lasers are observed experimentally on a PRO.

It is interesting to analyze the opposite limit of (14): the case when many transverse modes are active. This can be realized in experiments for both lasers and PRO's by using a resonator with plane (or almost plane) mirrors and a wide aperture. The LGLE then transforms to the complex Ginzburg-Landau equation (CGLE):

$$\frac{\partial E}{\partial \tau}=\left[\frac{n_s}{2}-1\right](1+i)E+id'\vec{\nabla}^2E-(1+i)|E|^2E\ . \qquad (19)$$

Here $d'=dn/2$.

The CGLE (19) is completely diffractive (that is, the coefficient of the Laplace operator is purely imaginary). This is a consequence of the fact that there is no diffusion term in the initial equations for the refractive index (7).

The analysis of the CGLE [32,33] allows then the calculation of the radius of the core of the vortices and thus the characteristic scale of the spatial structure in turbulence, which is $x_0^2\cong d'/(n_s/2-1)$. Using the definition of d' one obtains $x_0^2\cong\lambda L/T$.

This result is qualitatively compatible with the experimental observations in [34] that the spatial scale in the turbulent regime ceases to depend on the aperture radius (or Fresnel number) when the latter is larger than a critical value. This experimental observation was interpreted in [34] as due to a material property, namely, to diffusion of charges [adding a real part to the coefficient of the Laplace operator in (7)]. But the infinite spatial scale can already be explained (without invoking particular material properties) in the above sense that the structure results already from the equations. Of course, whether the "generic" diffractive or the "nongeneric" material-dependent scale dominates depends on the actual material used and on oscillator parameters such as the pump.

Diffusion tends to stabilize solutions, and defect-mediated turbulence does not occur in a CGLE with prevailing diffusion. The solutions of the CGLE have in this case been shown to be modulationally stable [32,33]. On the other hand, for the diffractive CGLE instabilities occur at a lower pump.

Thus the common observation of turbulence in PRO's would seem to indicate that these systems are rather more diffractive than diffusive and material properties are not so important. Correspondences with chemical systems therefore seem not so likely.

In addition, the dynamics of a vortex pair of opposite charges is different for a diffractive and a diffusive CGLE. In the diffusive case the vortices move straight towards one another, and annihilate. In the diffractive case they move parallel to one another (or around one another) [35]. Our qualitative experimental observations of the circling vortices hint at a more diffractive rather than diffusive dynamics.

ACKNOWLEDGMENTS

This work was supported by Deutsche Forschungsgemeinschaft and ESPRIT Project No. 7118 (TONICS). M. F. H. Tarroja acknowledges financial support from the Alexander von Humboldt Foundation. We also thank D. Hennequin for useful discussions.

[1] J.-L. de Bougrenet e la Tocnaye, P. Pellat-Finet, and J. P. Huignard, J. Opt. Soc. Am. B **3**, 315 (1986).
[2] D. Z. Anderson and R. Saxena, J. Opt. Soc. Am. B **4**, 164 (1987).
[3] A. Yariv and S.-K. Kwong, Opt. Lett. **10**, 454 (1985).
[4] P. Yeh, J. Opt. Soc. Am. B **2**, 1924 (1985).
[5] F. T. Arecchi, G. Giacomelli, P. L. Ramazza, and S. Residori, Phys. Rev. Lett. **65**, 2531 (1990).
[6] F. Laeri, T. Tschudi, and J. Albers, Opt. Commun. **47**, 387 (1983).
[7] G. Pauliat and P. Günter, Opt. Commun. **66**, 329 (1988).
[8] H. Rajbenbach and J. P. Huignard, Opt. Lett. **10**, 137 (1985).
[9] P. Pellat-Finet and J.-L. de Bougenet de la Tocnaye, Opt. Commun. **55**, 305 (1985).
[10] D. Hennequin, L. Dambly, D. Dangoisse, and P. Glorieux, J. Opt. Soc. Am. B **11**, 676 (1994).
[11] G. D'Alessandro, Phys. Rev. A **46**, 2791 (1992).
[12] L. Dambly and H. Zeghlache, Phys. Rev. A **47**, 2264 (1993).
[13] L. A. Lugiato, G.-L. Oppo, J. R. Tredicce, L. M. Narducci, and M. A. Pernigo, J. Opt. Soc. Am. B **7**, 1019 (1990).
[14] N. V. Kukhtarev, V. B. Markov, S. G. Odulov, M. S. Soskin, and V. L. Vinetskii, Ferroelectrics **22**, 940 (1979).
[15] P. Günter and H. J. Eichler, in *Electro-Optic and Photorefractive Materials,* Proceedings of the International School on Material Science and Technology, Erice, Italy, 1986, edited by P. Günter (Springer-Verlag, Berlin, 1987), pp. 206–228.
[16] M. D. Ewbank and P. Yeh, Opt. Lett. **10**, 496 (1985).
[17] (a) J. P. Huignard and A. Marrakchi, Opt. Commun. **38**, 249 (1981); (b) A. Marrakchi and J. P. Huignard, Appl. Phys. **24**, 131 (1981).
[18] P. N. Günter, Opt. Commun. **41**, 82 (1982).
[19] H. Rajbenbach, J. P. Huignard, and B. Loiseux, Opt. Commun. **48**, 247 (1983).
[20] G. C. Valley, J. Opt. Soc. Am. B **1**, 868 (1984).
[21] P. K. Jakobsen, J. V. Moloney, A. C. Newell, and R. Indik, Phys. Rev. A **45**, 8129 (1992).
[22] K. Staliunas, Phys. Rev. A **48**, 1573 (1993).
[23] K. Staliunas and C. O. Weiss, Physica D **81**, 79 (1995).
[24] A. B. Coates, C. O. Weiss, C. Green, E. J. D'Angelo, J. R. Tredicce, M. Brambilla, M. Cattaneo, L. A. Lugiato, R. Pirovano, F. Prati, A. J. Kent, and G.-L. Oppo, Phys. Rev. A **49**, 1452 (1994).
[25] K. Staliunas, C. O. Weiss, and M. F. H. Tarroja, Opt. Commun. **102**, 69 (1993).
[26] B. Baranova, B. Ya. Zel'dovich, A. V. Mamaev, N. F. Pi-

lipetskii, and V. V. Shumov, Sov. Phys. JETP **56**, 983 (1982).
[27] F. T. Arecchi, G. Giacomelli, P. L. Ramazza, and S. Residori, Phys. Rev. Lett. **67**, 3749 (1991).
[28] C. Tamm, Phys. Rev. A **30**, 5960 (1988).
[29] F. Prati, Ph.D. dissertation, University of Milano, 1992.
[30] C. O. Weiss, Phys. Rep. **219**, 311 (1992).
[31] W. Klische, C. O. Weiss, and B. Wellegehausen, Phys. Rev. A **39**, 919 (1989).
[32] P. Coullet, L. Gil, and J. Lega, Phys. Rev. Lett. **62**, 1619 (1989).
[33] I. S. Aranson, L. Kramer, and A. Weber, Physica D **53**, 376 (1991).
[34] F. T. Arecchi, S. Boccaletti, P. L. Ramazza, and S. Residori, Phys. Rev. Lett. **70**, 2277 (1993).
[35] S. Rica and E. Tirapequi, Phys. Rev. Lett. **64**, 878 (1990).

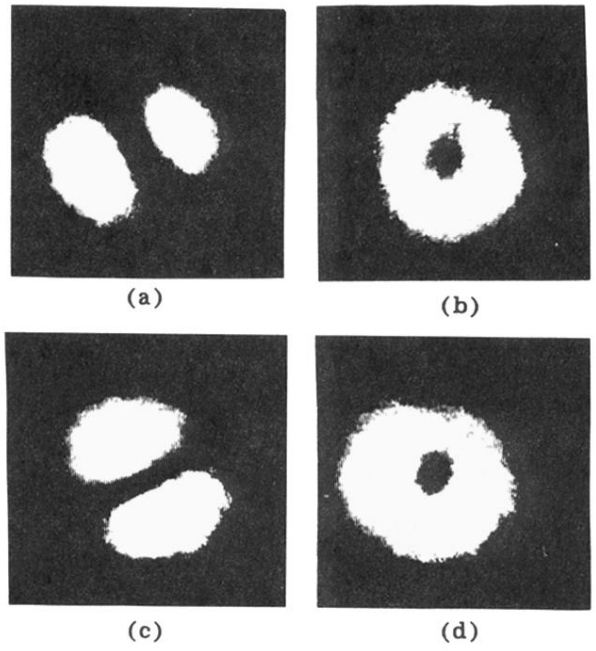

FIG. 10. The "unlocked doughnut." Output alternates between (a) Hermite 01 mode, (b) right-hand helical wave, (c) Hermite 10 mode, and (d) left-hand helical wave.

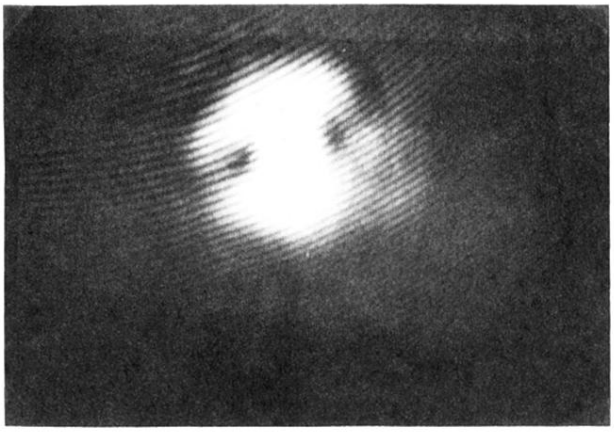

(a)

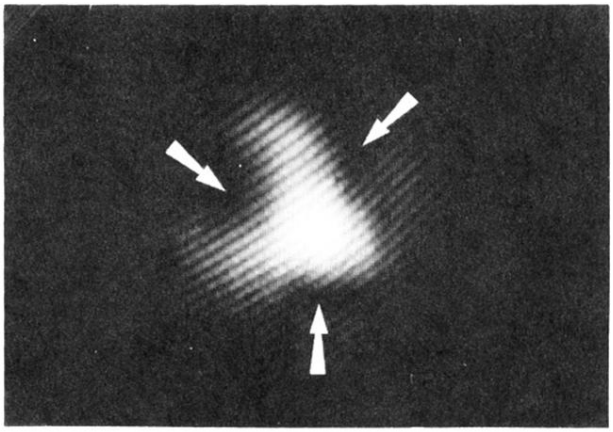

(b)

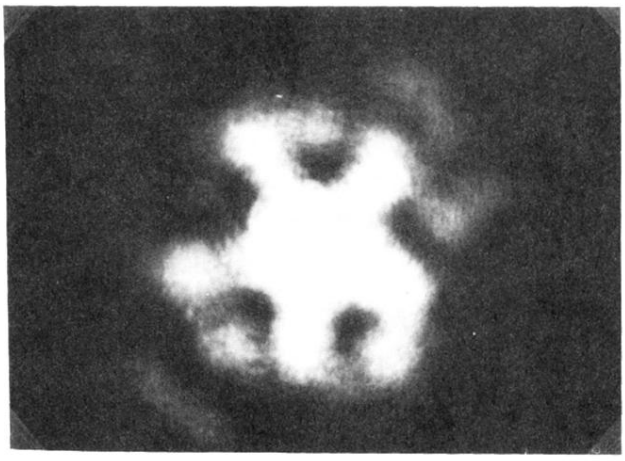

(c)

FIG. 11. Circling about the optical axis of (a) two vortices, (b) three vortices (indicated by arrows), and (c) five vortices. For (a) and (b) the emitted field is superimposed on part of the pump radiation to detect vortices.

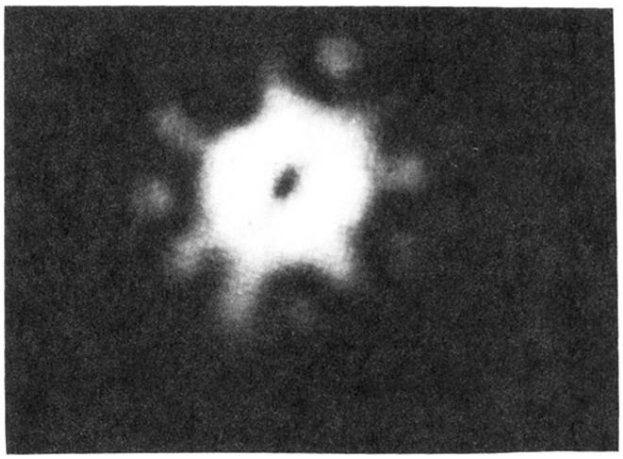

FIG. 12. Simultaneous emission of a $q = 1$ "doughnut mode" and a pattern of the $q = 6$ mode family.

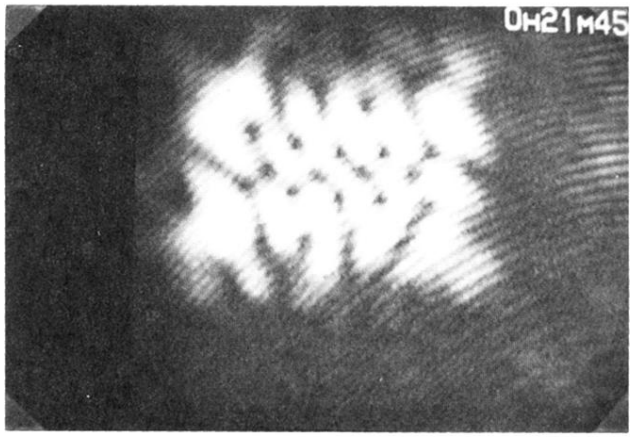

FIG. 13. A "vortex crystal." The fringes are due to interference with part of the pump beam (superposed to detect vortices).

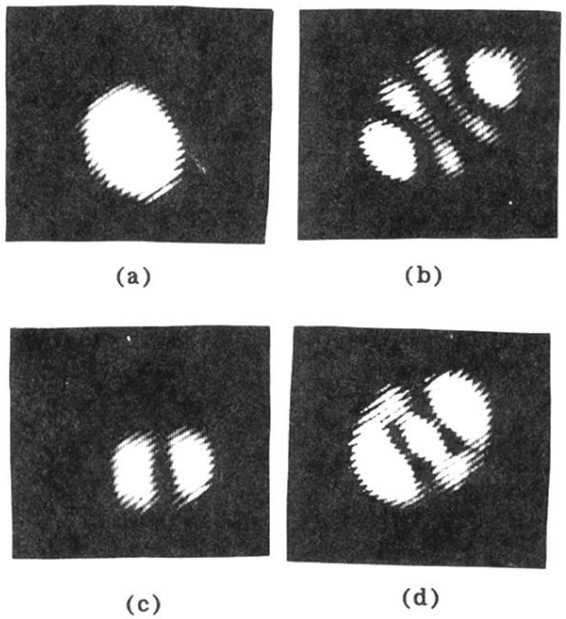

FIG. 9. Sequence of patterns observed when the resonator length is changed through one free spectral range (mode families up to $q=3$ are allowed to oscillate). Only one representative pattern for each mode family is shown. (a) $q=0$, (b) $q=3$, (c) $q=1$, and (d) $q=2$. The fringes are due to interference with the pump beam (superimposed to detect vortices).